Phenylazothiazoles as Visible-Light Photoswitches

Runze Lin,[a, b ‡] P. K. Hashim, [a, b ‡] Saugata Sahu,[a] Ammathnadu S. Amrutha,[a, b] Nusaiba Madappuram Cheruthu,[a, b] Shakkeeb Thazhathethil,[a, b] Kiyonori Takahashi,[a, c] Takayoshi Nakamura,[a, c] Takashi Kikukawa,[b, d] and Nobuyuki Tamaoki* [a, b]

[a] Research Institute for Electronic Science, Hokkaido University, Kita20, Nishi 10, Kita-ku, Sapporo, Hokkaido, 001-0020, Japan.

[b] Graduate School of Life Science, Hokkaido University, Kita 10, Nishi 8, Kita-ku, Sapporo, Hokkaido, 060-0810, Japan.

[c] Graduate School of Environmental Science, Hokkaido University, Kita 10, Nishi 5, Kita-ku, Sapporo, Hokkaido, 060-0810, Japan.

[d] Faculty of Advanced Life Science, Hokkaido University, Sapporo, 060-0810, Japan

ABSTRACT: A novel class of photoswitches based on a phenylazothiazole scaffold that undergoes reversible isomerization under visible-light irradiation is reported. The photoswitch, which comprises a thiazole heteroaryl segment directly connected to a phenyl azo chromophore, has very different spectral characteristics, such as a redshifted absorption maximum wavelength and well-separated absorption bands of the *trans* and *cis* isomers, than conventional azobenzene and other heteroaryl azo compounds. Substituents at the *ortho* and *para* positions of the phenyl ring of the photoswitch resulted in a further shift to longer wavelengths up to 525 nm at the absorption maximum with a small thermal stability compensation. These photoswitches showed excellent photostationary distributions of the *trans* and *cis* isomers, thermal half-lives of up to 7.2 h, and excellent reductant stability. The X-ray crystal structure analysis revealed that the *trans* isomers exhibited a planar geometry, and the *cis* isomers exhibited a T-shaped orthogonal geometry. Detailed *ab initio* calculations further demonstrated the plausible electronic transitions and isomerization energy barriers, which were consistent with the experimental observations. The fundamental design principles elucidated in this study will aid in the development of a wide variety of visible-light photoswitches for photopharmacological applications.

INTRODUCTION

Azo-based photoswitches absorb specific wavelengths of light and undergo reversible conversion between their *trans* (*E*) and *cis* (*Z*) isomers, which have been utilized for diverse applications in material science,[1–7] biology,[8–11] and pharmacology.[12–15] The performance of a photoswitch is determined based on distinct factors such as the absorption maximum wavelength (λ_{max}), quantum yield (Φ), relative abundance of *E* and *Z* isomers at the photostationary state (PSS), thermal stability of the isomers, and fatigue-resistant photoswitching cycle.[16] For conventional azobenzene photoswitches, one method for tuning the spectral characteristics and thereby altering photoswitch properties is to substitute suitable functional groups on the phenyl rings.[17–24] "Heteroaryl azo"–based photoswitches have recently received considerable attention owing to their photophysical characteristics originating from the heterocyclic aryl motifs.[25] Photoswitches with a five-membered heteroaryl motif exhibit distinct photophysical properties, steric profiles, and molecular geometries.[26–29] Many drug molecules possess a five-membered heteroaryl motif;[30–33] hence, their photoswitchable analogs can be used in the field of photopharmacology, provided that the photoswitch isomerizes when exposed to visible light.[34,35] Pyrrole, pyrazole, imidazole, isoxazole, triazole, and thiophene are considered as the five-membered heteroaryl motifs that have been used in the development of photoswitches.[36–42] Some of these photoswitches have shown exceptionally long half-lives;[36, 40b] however, they require ultraviolet (UV)-light irradiation for *E*→*Z* isomerization.

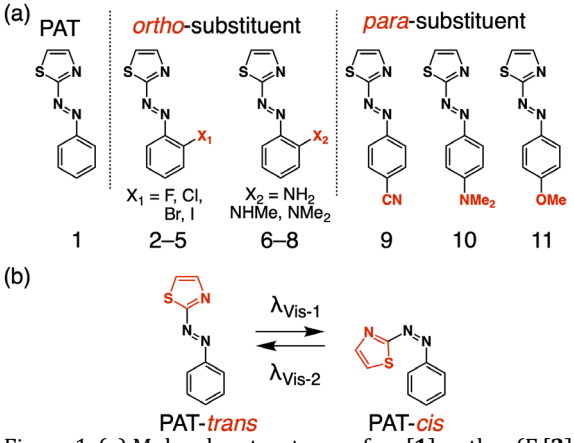

Figure 1. (a) Molecular structures of un [**1**], ortho- (F [**2**], Cl [**3**], Br [**4**], I [**5**], NH_2 [**6**], NHMe [**7**], NMe_2 [**8**]) and para- (CN [**9**], NMe_2 [**10**], OMe [**11**]) substituted **PAT**. (b) Scheme showing the reversible isomerization of **1** using visible-light irradiation having different wavelengths.

Scheme1. Synthesis of PAT photoswitches

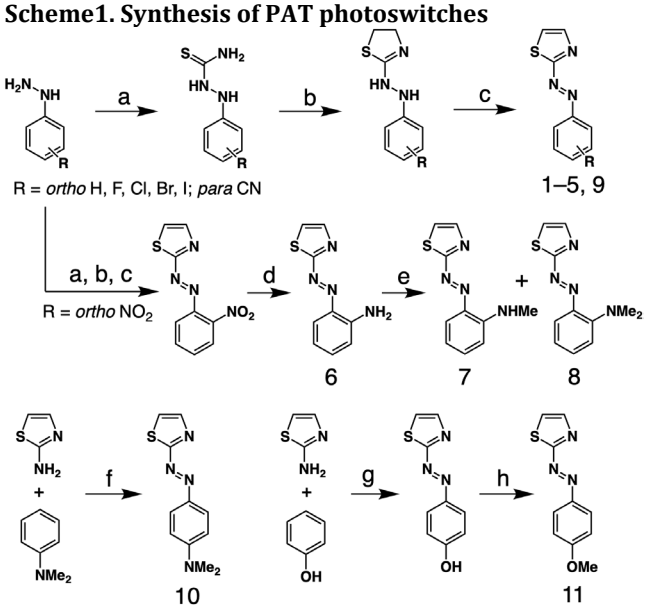

Reagents and conditions. (a) NH_4SCN, $EtOH/H_2O$ (9:1 v/v), 25°C; (b) $BrCH_2CH_2NH_2{\cdot}HBr$, iPrOH, 110°C, then $NaHCO_3$; (c) Na_2CO_3 [or Ag_2O], EtOH, 110°C; (d) Zn, NH_4Cl, MeOH, 25°C; (e) MeI, DMF, 30°C (f) Concentrated H_2SO_4, $NaNO_2$, 0°C (g) Concentrated HCl, aqueous $NaNO_2$, 0°C; (h) K_2CO_3, DMF, then dimethyl sulfate, 25°C.

In the case of thiophene-based photoswitches, both *E*→*Z* (365 nm) and *Z*→ *E* (285 nm) isomerizations require UV irradiation.[42] Conversely, azobenzazoles can be isomerized using visible light, albeit with relatively short half-lives of the *Z* isomers (e.g., 0.4 s for benzothiazole).[43,44] Our interest was to investigate novel thiazole-based photoswitches as a new class of "heteroaryl azo" compounds with isomerization induced by visible light and relatively long half-lives of the *Z* isomers. Previously, a visible-light switchable p38α kinase inhibitor comprising 4,5-disubstituted phenylazothiazole (**PAT**) was reported; however, the azo moiety was reduced to hydrazine in the presence of dithiothreitol (DTT).[45] We recently reported a visible-light switchable Rho kinase inhibitor based on a pyridine-appended **PAT** that was stable in the presence of DTT and glutathione.[46] Motivated by this finding, in the present study, we focused on the fundamental properties and substituent effects of **PAT** compounds, aiming to establish a new category of visible-light photoswitches. We envisioned that the electron-donating sulfur heteroatom of thiazole should have a favorable effect to reduce the energy gap of π→π* transitions, enabling isomerization via visible-light absorption. We indeed found that **PAT** photoswitches generally isomerize reversibly under visible-light irradiation, resulting in an excellent composition of *E* and *Z* isomers at the PSS and reasonably long thermal half-lives of the *Z* isomers.

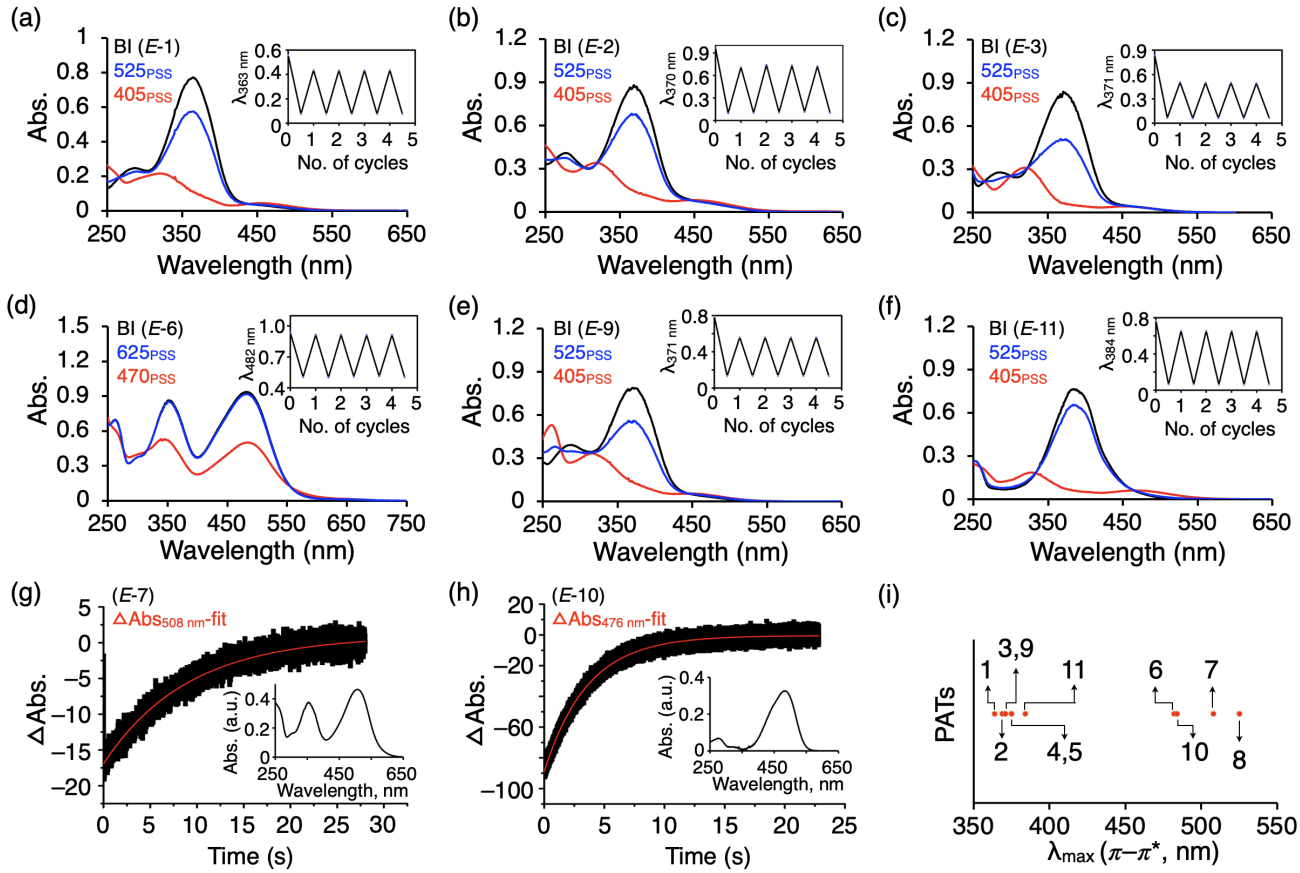

Figure 2. (a–f) UV–visible absorption spectra of **1–3, 6, 9,** and **11** in acetonitrile at 25°C before irradiation (BI, black lines), the PSS of 405 nm or 470 nm (405_{PSS}, 470_{PSS}, red lines) and 525 nm or 625 nm irradiation (525_{PSS}, 625_{PSS}, blue lines). Absorbance changes at λ_{max} obtained by repeated irradiation at the PSS (insets). (g, h) Absorbance changes of **7** and **10** at 508 nm and 476 nm, respectively, obtained using laser flash photolysis (fit, red curve). (i) Graph of λ_{max} values of **1–11** showing the shift of their λ_{max} to longer wavelengths.

Interestingly, electron-donating or withdrawing substituents at the *ortho* or *para* positions on the phenyl ring of the photoswitch compound resulted in a further shift of the λ_{max} to longer wavelengths with a smaller thermal stability compensation effect for some **PAT** derivatives. We also demonstrated the unusual T-shaped geometry of the *Z* isomer of **PAT** using X-ray crystal analysis. In addition, **PAT** photoswitches without strong electron-withdrawing substituents showed excellent stability against DTT and glutathione reductants.

RESULTS AND DISCUSSION

Synthesis and photoswitch properties. We synthesized compounds **1**–**5** and **9** from the corresponding phenyl hydrazine hydrochlorides via thiazoline cyclization followed by oxidation.[47] The yield (<10%) of the oxidation reaction of 4,5-dihydrothiazole to azothiazole was enhanced (>30%) using silver dioxide as the oxidizing agent instead of air. For **6**–**8**, a nitro-appended **PAT** derivative was selectively reduced to an amine using zinc, which was then methylated using methyl iodide. Compounds **10** and **11** were synthesized from aminothiazole via a direct azo coupling reaction (Scheme 1 and S1–S4). The compounds were unambiguously characterized using a variety of analytical methods (^{1}H NMR, ^{13}C NMR, and mass spectroscopy; Figures S1–S33). The synthesis of **1** was reported previously without any study on its photophysical properties.[47] We studied the photoswitching ability of **PAT** derivatives using absorption spectroscopy in acetonitrile solution at 25°C (Figures 2 and S43–S49). As synthesized **1** exhibited two absorption bands (λ_{max} = 364 and 459 nm) assignable to the π→π* and n→π* electronic transitions, respectively. The λ_{max} value (π→π*) of the *E* isomer of **1** was redshifted by ∼47 nm compared with the *E* isomer of azobenzene (Figure S34). Owing to the redshifted spectral features of **1**, we could induce photoisomerization using visible-light irradiation. Under 405 nm light irradiation, the absorption band intensities were considerably altered to reach the PSS (405_{PSS}) with 83% *Z* isomers (determined using ^{1}H NMR; Figure S35 and Table 1). The *E*→*Z* isomerization also occurred under 430 nm light irradiation, although with a reduced *Z* isomer composition (∼52%) at the PSS (Figure S43). Under 525 nm light irradiation (525_{PSS}), an opposite trend was observed for the change in the absorption bands, resulting in an *E* isomer composition of 81% (Figure 2a). We then studied the effect of substituents at the *ortho* or *para* positions on the phenyl component of **PAT**. Electron-withdrawing F, Cl, Br, I, and CN substituents marginally affected the absorption spectra of **2**–**5**, and **9**, respectively, with a slight red-shift in the λ_{max} values compared with **1** (Table 1), and the compounds underwent reversible photoisomerization similar to that of parent **1** (Figures 2b–e, S36–S46, and Table 1). Interestingly, **3** and **4** with bulky Cl and Br at the phenyl *ortho* positions, respectively, presented highly efficient *E*→*Z* photoisomerization compared with **1**, resulting in 96% *Z* isomers at 405_{PSS} (Figures 2c and S44). However, the n→π* spectral band of the *Z* isomers partially overlapped with that of the *E* isomers, causing less efficient *Z*→*E* photoisomerization and providing only 65% *E* isomers at 525_{PSS} (Figure 2c and Table 1). The electron-donating NH_2 (**6**), NHMe (**7**), NMe_2 (**8** and **10**), and OMe (**11**) substituents considerably affected the absorption spectra, with a 20–161 nm red-shift in the λ_{max} values compared with **1** (Figure 2i). Importantly the *E*→*Z* and *Z*→*E* photoisomerizations occurred under longer wavelengths of 470 or 525 nm and 625 nm light irradiation, respectively, for **6**, **7**, and **10** (Figures 2d, S47, and S48). Because of the fast thermal relaxation kinetics of **7** and **10**, we

Table 1. Spectral and kinetic data for 1–11.

PAT	π–π^* (*E*)		n–π^* (*E*)		Conversion (%)		$t_{1/2}$ (25 °C)	E_a	$\Delta H^‡$	$\Delta S^‡$	$\Delta G^‡$ (25 °C)	∅	∅
	λ_{max} nm	ε M^{-1} cm^{-1}	λ_{max} nm	ε M^{-1} cm^{-1}	*E*→*Z* (405 nm)	*Z*→*E* (525 nm)	h	kJ mol^{-1}	kJ mol^{-1}	J mol^{-1} K^{-1}	kJ/mol	*E*→*Z*	*Z*→*E*
1	364	19723	459	769	85	81	2.8	87.9	85.4	–38.4	96.8	0.24	0.78
2	369	18592	458	969	90	77	5.5	94.2	91.7	–20.8	97.9	0.31	0.43
3	371	12738	471	692	96	62	6.6	94.5	92.0	–23.0	98.8	0.45	0.31
4	375	14903	477	666	96	62	7.2	90.5	88.0	–37.7	99.3	0.27	0.44
5	375	12521	498	389	91	72	3.6	86.8	84.4	–43.8	97.4	0.17	0.61
6	351 482	9788 10895	–	–	>58* (470 nm) >48* (525 nm)	>97* (625 nm)	45 s	76.1	73.1	–32.7	83.4	–	–
7	353 508	11262 14591	–	–	>37* (470 nm) >41* (525 nm)	>89* (625 nm)	6 s	–	–	–	–	–	–
8	365 525	3675 3278	–	–	–	–	–	–	–	–	–	–	–
9	371	23049	468	653	88	76	1.7	74.6	72.2	–78.6	95.6	0.21	0.71
10	484	28830	–	–	>68* (470 nm) >52* (525 nm)	>99* (625 nm)	2 s	–	–	–	–	–	–
11	384	25944	–	–	>92	86	0.25	80.8	78.3	–41.6	90.7	0.34	–

* Conversion at the PSS was estimated based on the NMR results except for **6**, **7**, **10**, and **11**, for which the absorbance spectra were used. Half-life was calculated from the absorbance changes at thermal *Z*–*E* isomerization except for **7** and **10**, for which laser flash photolysis was used.

also conducted laser flash photolysis, which showed a sudden decrease in absorbance at 508 nm (for **7**) and 476 nm (for **10**) and an increase in absorbance at 550 nm (for **10**) followed by a slow recovery of the original absorbance (Figures 2g, 2h, and S50). To our surprise, **11** showed the best forward E⟶Z (92%) and reverse *Z*→*E* (88%) photoisomerization abilities, which is probably attributable to the optimum spectral separation of the π→π* ($\Delta\lambda_{max}$ = 53 nm) and n→π* ($\Delta\lambda_{max} \cong$ 5 nm) transition bands of the *E* and *Z* isomers, respectively (Figure S42 and Table 1). Compounds **1–6**, **9**, and **11** underwent reversible *E*→*Z* photoisomerization for many cycles with no degradation, indicating high fatigue resistance (Figures 2a–2f insets), which is required for photopharmacological applications. However, **8** with NMe_2 substituents at the phenyl *ortho* position decomposed after light irradiation (Figure S49). We measured the quantum yields (Φ) of **1–5**, **9**, and **11** at 405 nm for the *E*→*Z* photoisomerization using ferrioxalate actinometry. For the *Z*→*E* photoisomerization, the Φ values were calculated to be in the ranges of 0.17–0.45 (*E*→*Z*) and 0.31–0.78 (*Z*→*E*) (Tables 1 and S1–S7 and Figures S51–S62). The half-lives of the *Z* isomers and the *Z*→*E* thermal isomerization kinetics were studied using absorption spectroscopy or laser flash photolysis in acetonitrile solution at 25°C (Table 1). Compounds **1–6**, **9**, and **11** followed first-order thermal isomerization kinetics, and their half-lives ($t_{1/2}$) were calculated from the rate constants (Table 1 and Figures S63–S118). We observed a reasonably stable *Z* isomer of parent **1** ($t_{1/2}$ = 2.8 h) and a destabilization effect when the electron-donating OMe substituent was present, as in the case of **11** ($t_{1/2}$ = 14.8 min). In contrast, electron-withdrawing halogen substituents at the phenyl *ortho* position further stabilized the *Z* isomers. Compound **4** with a Br substituent showed the longest half-life ($t_{1/2}$ = 7.2 h) among all the **PAT** photoswitches studied (Table 1). Interestingly, despite its strong electron-withdrawing character, the *Z* isomer of **9** with CN substituents at the phenyl *para* position destabilized ($t_{1/2}$ = 1.7 h) compared with parent **1** (Table 1). Importantly, the $t_{1/2}$ values for the *Z* isomers of **6**, **7**, and **10** were 45, 6, and 2 s, respectively, which were much longer than those of green-light switchable azobenzene derivatives. For instance, the $t_{1/2}$ value of the *Z* isomer of 4-dimethylamino-4'-nitroazobenzene, which isomerizes when exposed to >470 nm irradiation, is in the order of milliseconds.[48] Compounds **6**, **7**, and **10** underwent *E*→*Z* photoisomerization when exposed to 525 nm irradiation, but their $t_{1/2}$ values were in the order of seconds. To maintain a *Z*-rich state in photophamacological applications, no light irradiation or less frequent flashes are enough for compounds with *Z* isomers showing $t_{1/2}$ values in the order of hours or tens of minutes, whereas continuous irradiation of an active light is necessary for those showing $t_{1/2}$ values in the order of seconds. The activation energy (E_a), enthalpy ($\Delta H^{\ddagger}$), entropy ($\Delta S^{\ddagger}$), and Gibbs free energy ($\Delta G^{\ddagger}$) were determined using the Arrhenius and Eyring plots of the *Z*→*E* thermal isomerization kinetics in acetonitrile solution at five different temperatures (5°C – 35°C) (Table 1 and Figures S63–S118).

The effect of water in the solvent on the photophysical and thermal isomerization properties was also studied for **1**, **6**, **7**, and **11**. Although the water in the media had little effect on **1** and **11**, the $t_{1/2}$ values of **6** and **7** with amino substituents decreased after changing the solvent from acetonitrile to an acetonitrile/water (50/50, v/v) mixture (Figure S119 and Table S8).

X-ray single-crystal structures. For a deeper understanding regarding the molecular geometry of PAT photoswitches, we examined the X-ray single-crystal structures of the *E* and *Z* isomers. The *E* isomers of **1** and **3** adopted a conformation in which the phenyl and thiazole parts were coplanar (Figure 3a), as in the case of azobenzene. However, the *Z* isomers adopted an unusual T-shaped conformation with orthogonal geometry of the two aromatic rings in which the S atom of thiazole was facing the phenyl aromatic ring. This is in sharp contrast to the *Z* isomer of azobenzene, which possesses a twisted geometry in the two phenyl rings

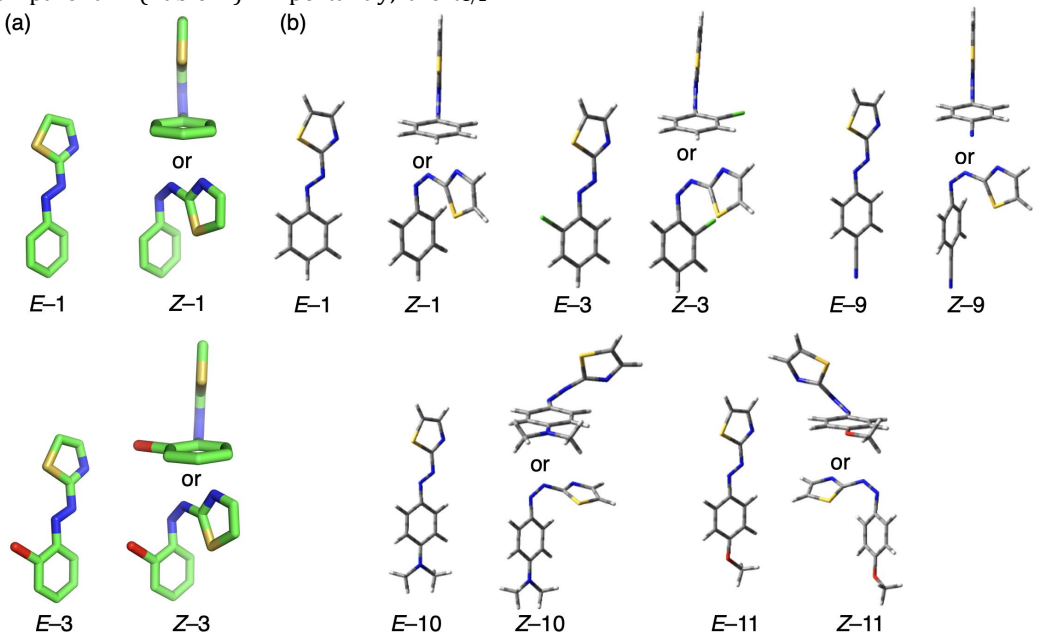

Figure 3. (a) Single-crystal X-ray structures of both *E* and *Z* isomers of **1** and **3** (green = C; blue = N; golden = S; red = Cl). Hydrogens are omitted for clarity. (b) Geometry optimized calculated conformations of *E* and *Z* isomers of **1**, **3**, **9**, **10**, and **11**.

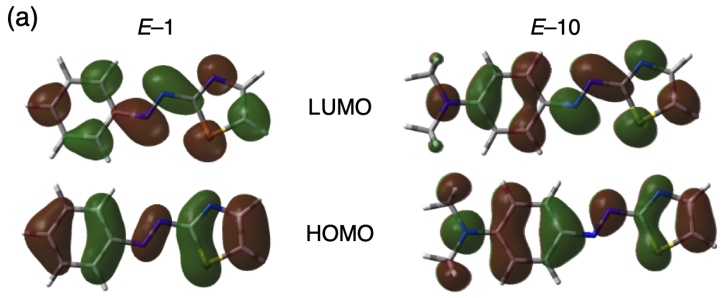

(b)

		Phenyl (%)	N=N (%)	Thiazole (%)
E–1	LUMO	21	46	33
	HOMO	32	14	55
E–10	LUMO	29	39	30
	HOMO	62	11	19

Figure 4. (a) LUMO, HOMO, and HOMO-1 of *E*-**1** and *E*-**10.** (b) HOMO and LUMO electron distributions at different groups having π and π* natures (phenyl, N=N, and thiazole units) in *E*-**1** and *E*-**10**.

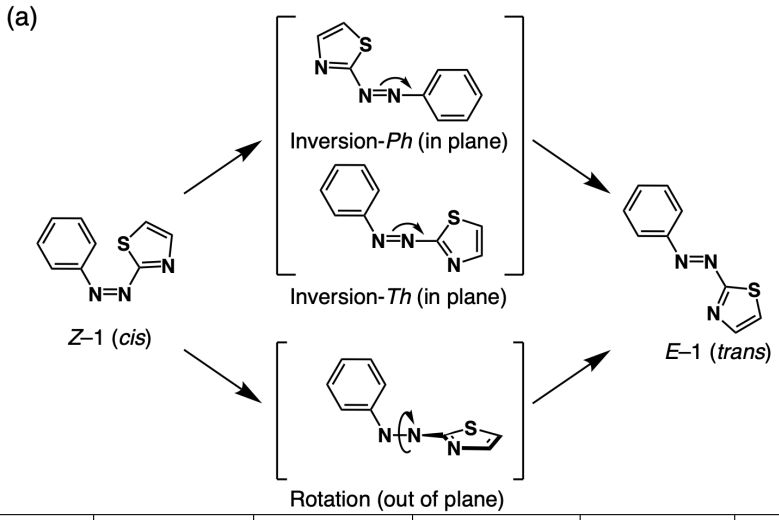

(b)

PATs	1	3	9	10	11
Transition state	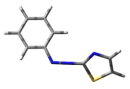	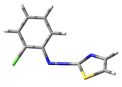	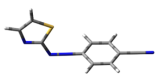	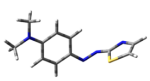	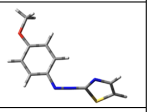
Isomerization pathway	Inversion-*Th*	Inversion-*Th*	Inversion-*Ph*	Rotation	Inversion-*Th*
E_a^{cal} (kJ mol^{-1})	94.06	99.76	86.50	67.86	88.14

Figure 5. (a) Scheme showing the inversion and rotation pathways for the isomerization of 1. (b) Transition states and calculated activation energies (E_a^{cal}) of PAT derivatives.

are twisted. Although calculations have predicted this type of perfect T-shaped conformation in the *Z* isomer of some heteroaryl azo compounds, this has not been demonstrated experimentally.[38, 42] In our case, the X-ray crystal structure of *Z*–**1** clearly showed a perfect T-shaped conformation with a dihedral angle of 89.7°(Phenyl-CNNC). For *Z*–**3** with a bulky Cl substituent, the dihedral angle for Phenyl-CNNC was 98.4°, which slightly deviated from the T-shaped conformation (Figure 3a).

Theoretical calculations. To gain further insights into the molecular structures, molecular orbital energy levels, and energy barriers for isomerization, we performed density functional theory (DFT) calculations using a 6-31+G(d,p) basis set with Becke's three-parameter hybrid exchange and the Lee–Yang–Parr correlation functional (B3LYP)

including the Grimme dispersion correction in acetonitrile medium. The most stable optimized geometry in the ground state of both the *E* and *Z* isomers of **1, 3, 9, 10**, and **11** are shown in Figure 3b and Tables S9–S18, and the less stable conformers are shown in Figure S120. A planar geometry was observed in the *E* isomers of **1**, **3**, **9**, **10**, and **11** with the phenyl, azo, and thiazole moieties in the same plane. However, in the *Z* isomers of the same **PAT** derivatives (**1**, **3**, and **9**), an orthogonal geometry was observed with the S atom of the thiazole ring facing the phenyl ring (Figure 3b). For *Z*–**1** and *Z*–**3**, the X-ray crystal structure analysis unambiguously revealed the orthogonal geometry with the S atom of the thiazole ring facing the phenyl ring. In contrast, the calculated conformers of *Z*–**10** and *Z*–**11** showed a twisted conformation (Figures 3b and S121). This calculation result and the X-ray crystal structures of the *Z* isomers are explained as follows: the origin of the attractive force stabilizing the T-shaped conformation in *Z*–**1** and *Z*–**3** was the electron transfer from the S lone pair to the π* antibonding orbital in the phenyl ring. This effect was weakened in *Z*–**10** and *Z*–**11** with electron-donating NMe_2 and OMe substituents, respectively.[49, 50] The n-orbital of the S atom extended farther than that of the N atom, which explains the favored orientation of the thiazole in the T-shaped conformer with the S atom rather than the N atom facing the phenyl ring, which provides a π* orbital on the ring plane.

We then simulated the theoretical absorption spectra of both the *E* and *Z* isomers of **1**, **3**, **9**, **10**, and **11** in acetonitrile, which showed strong π→π* and weak n→π* electronic transitions (Figure S122). For instance, the λ_{max} of the calculated spectra of *E*–**1** appeared at 397 nm (oscillatory strength (f) = 0.704) and 477 nm (f = 0.000), whereas that of *Z*–**1** appeared at 350 nm (f = 0.024) and 502 nm (f = 0.001). The λ_{max} (π–π*) of the substituted **PAT** (*E*–**3** (411 nm), *E*–**9** (412 nm), *E*–**10** (475 nm), and *E*–**11** (430 nm)) was further red-shifted compared with the parent **PAT** (*E*–**1** (397 nm)), which was similar to the trend observed in the experimental spectra. The relative intensities of the n→π* transitions of *Z*–**10** ($f_{527\ nm}$ = 0.202) and *Z*–**11** ($f_{529\ nm}$ = 0.113) were much higher than that of *Z*–**1** ($f_{502\ nm}$ = 0.001). The n→π* transition was symmetry-allowed for *Z*–**10** and *Z*–**11** because of their twisted orthogonal geometry, but symmetry-forbidden for *Z*–**1**.[38] The experimentally obtained molar extinction coefficient (ε) of *Z*–**11** corresponding to the n→π* transition was 2044 $M^{-1}cm^{-1}$. The n→π* transition at 550 nm in the calculated absorption spectra of *Z*–**10** was supported by the flash photolysis results, in which a sudden increase in the absorbance at 550 nm was observed (Figure S50). Figure 4 shows the frontier molecular orbitals and the electron distribution at each group in the *E* isomers of **1** and **10**. The highest occupied molecular orbital (HOMO), lowest unoccupied molecular orbital (LUMO), and HOMO-1 have a π, π*, and n nature, respectively.[51] During the π→π* transition, the electron density of thiazole decreases more than that of phenyl, whereas that of the azo group increases. The nature of this intramolecular charge transfer from electron-rich thiazole to azo upon the π→π* transition of **1** could be the origin of the red-shift in absorbance compared with azobenzene.[52] An enormous electron-density shift from the NMe_2-substituted phenyl to azo and to thiazole is observed in **10**, which contributes to its further red-shift in the π→π* transition band.

We then calculated the potential energy diagrams for the *Z*→*E* isomerization using the B3LYP/6-31+G(d,p) level of theory. To determine the preferred thermal isomerization pathway, we calculated the activation energies for the inversion and rotation pathways separately (Figures S123–S125). The inversion pathway can occur either via the azo phenyl (inversion-*Ph*) or azo thiazole (inversion-*Th*) segments. The obtained relative energies of the *Z* isomers of **1**, **3**, **10**, and **11** were 62–75 kJ mol^{-1} higher than those of the *E* isomers, indicating

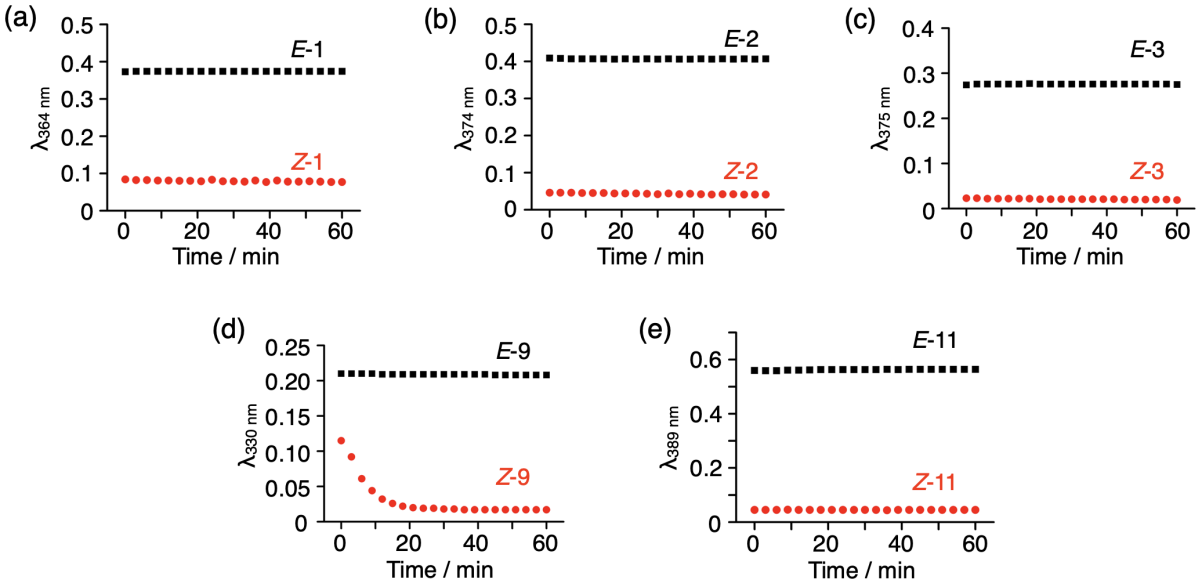

Figure 6. Absorbance changes of **1–3**, **9,** and **11** (20 μM) over time after incubation for 60 min at 25°C in aqueous solution (BRB80 buffer: acetonitrile = 1:1 v/v) containing glutathione (1 mM) reductant. The black squares and red circles represent the absorbance before and after 405 nm light irradiation, respectively, followed by a 3-min incubation period before each measurement.

the reduced stability of the *Z* isomer than the *E* isomer (Figure S123). We found that **1**, **3**, and **11** isomerized via inversion-*Th*, whereas **9** isomerized via inversion-*Ph*. Interestingly, **10** isomerized via the rotation of the azo segment (Figure 5a and Table S8). The calculated potential energy barriers for the *Z*→*E* thermal isomerization ($\Delta E_{Z\rightarrow E}$) of **10** (67.86 kJ mol^{-1}) and **11** (88.14 kJ mol^{-1}) having electron-donating NMe_2 and OMe substituents, respectively, were much lower than that of **1** (94.06 kJ mol^{-1}) (Figure 5b). The calculated activation energies (E_a^{cal}) for the *Z*→*E* thermal isomerization followed a similar trend as the experimentally obtained activation energies (Table 1).

Reductive stability. For biological applications, the photoswitch should be stable in a reductive environment such as cell cytoplasm. Reductants such as DTT and glutathione may react at the azo moiety of the photoswitch resulting in hydrazine. We tested the stability of **1–3**, **9**, and **11** by incubating them in a mixture of BRB80 buffer and acetonitrile (50/50, v/v) containing DTT (0.1 mM) or glutathione (1 mM) reductants. The absorbance spectra were then measured before and after light irradiation (Figure 6 and S126). Interestingly, the absorbance originating from the azo chromophore remained unchanged, indicating the excellent stability of the *E* and Z isomers of **PAT**s toward both DTT and glutathione reductants. However, the *Z* isomer of **9** with an electron-withdrawing CN group was unstable (Figure 6d).

CONCLUSIONS

We have demonstrated a novel class of five-membered "heteroaryl azo" photoswitches that reversibly isomerize on being exposed to visible light. The photoswitch with thiazole directly connected to a phenyl azo chromophore showed very different spectral characteristics than conventional azobenzene and other heteroaryl azo compounds. For instance, the λ_{max} value ($\pi\rightarrow\pi^*$) of **1** was 363 nm, which is 47 nm and 35 nm redshifted compared with those of azobenzene and azopyrazole, respectively.[29] Furthermore, the spectral band attributed to the *E* and *Z* isomers of **1** was redshifted, allowing us to reversibly isomerize the photoswitch using visible-light (405 and 525 nm) irradiation, providing an excellent *E* and *Z* isomer ratio at the PSS and a long thermal half-life of the *Z* isomer. The photoswitch properties (λ_{max}, $t_{1/2}$, and the PSS ratio) of **PAT** can be further tuned by introducing *ortho* and *para* substituents at the phenyl ring. In particular, **6**, having an *ortho* NH_2 substituent, showed reversible photoisomerization under longer wavelength visible light (525 and 625 nm) irradiation with a smaller thermal stability compensation effect and a longer half-life than visible-light switchable azobenzenes. Furthermore, **PAT** photoswitches showed excellent stability in the presence of reductants. Our calculation studies supported the experimental observations of the molecular energy parameters as well as the molecular geometries in both the *E* and *Z* isomers of the **PAT** photoswitches. We believe that the **PAT** class of photoswitches will provide unique applications, particularly in areas for which visible light is a requirement such as photopharmacology.[53] Such studies are currently underway.

ASSOCIATED CONTENT

Supporting Information

The Supporting Information is available free of charge on the ACS Publications website.

Experimental procedures for the synthesis of **1**–**11**, NMR, X-ray diffraction, and mass spectra, graphs used for the estimation of kinetic parameters (k, $t_{1/2}$, $\Delta S^{\ddagger}$, $\Delta H^{\ddagger}$, $\Delta G^{\ddagger}$), and DFT calculations (PDF).

AUTHOR INFORMATION

Corresponding Author

* tamaoki@es.hokudai.ac.jp

Author Contributions

‡These authors contributed equally and deserve to be considered as the first authors.

Funding Sources

This work was financially supported by KAKENHI Grants-in-Aid for Scientific Research B (22H02153) to NT.

ACKNOWLEDGMENT

R. L. acknowledges the Hokkaido University DX Doctoral fellowship. P. K. H. acknowledges the 8th Hokkaido University Interdepartmental Symposium Research Grant Silver Award.

REFERENCES

(1) Göstl, R.; Senf, A.; Hecht, S. Remote-controlling chemical reactions by light: Towards chemistry with high spatio-temporal resolution. *Chem. Soc. Rev.* **2014**, *43*, 1982–1996.

(2) Baroncini, M.; Silvi, S.; Credi, A. Photo- and redox-driven artificial molecular motors. *Chem. Rev.* **2020**, *120*, 200–268.

(3) Beharry, A. A.; Woolley, G. A. Azobenzene photoswitches for biomolecules. *Chem. Soc. Rev.* **2011**, *40*, 4422–4437.

(4) Klajn, R. Spiropyran-based dynamic materials. *Chem. Soc. Rev.* **2014**, *43*, 148–184.

(5) Zhang, Z.; Wang, W.; O'Hagan, M.; Dai, J.; Zhang, J.; Tian, H. Stepping out of the blue: From visible to near-IR triggered photoswitches. *Angew. Chem. Int Ed Engl* **2022**, *61*, e202205758.

(6) Pianowski, Z. L. Recent implementations of molecular photoswitches into smart materials and biological systems. *Chemistry* **2019**, *25*, 5128–5144.

(7) Goulet-Hanssens, A.; Eisenreich, F.; Hecht, S. Enlightening materials with photoswitches. *Adv. Mater.* **2020**, *32*, e1905966.

(8) Cheng, H.; Yoon, J.; Tian, H. Recent advances in the use of photochromic dyes for photocontrol in biomedicine. *Coord. Chem. Rev.* **2018**, *372*, 66–84.

(9) Welleman, I. M.; Hoorens, M. W. H.; Feringa, B. L.; Boersma, H. H.; Szymański, W. Photoresponsive molecular tools for emerging applications of light in medicine. *Chem. Sci.* **2020**, *11*, 11672–11691.

(10) Volarić, J.; Szymanski, W.; Simeth, N. A.; Feringa, B. L. Molecular photoswitches in aqueous environments. *Chem. Soc. Rev.* **2021**, *50*, 12377–12449.
(11) Thayyil, S.; Nishigami, Y.; Islam, M. J.; Hashim, P. K.; Furuta, K.; Oiwa, K.; Yu, J.; Yao, M.; Nakagaki, T.; Tamaoki, N. Dynamic control of microbial movement by photoswitchable ATP antagonists. *Chemistry* **2022**, *28*, e202200807.
(12) Velema, W. A.; Szymanski, W.; Feringa, B. L. Photopharmacology: Beyond proof of principle. *J. Am. Chem. Soc.* **2014**, *136*, 2178–2191.
(13) Broichhagen, J.; Frank, J. A.; Trauner, D. A roadmap to success in photopharmacology. *Acc. Chem. Res.* **2015**, *48*, 1947–1960.
(14) Hüll, K.; Morstein, J.; Trauner, D. In vivo photopharmacology. *Chem. Rev.* **2018**, *118*, 10710–10747.
(15) Hammerich, M.; Schütt, C.; Stähler, C.; Lentes, P.; Röhricht, F.; Höppner, R.; Herges, R. Heterodiazocines: Synthesis and photochromic properties, trans to cis switching within the bio-optical window. *J. Am. Chem. Soc.* **2016**, *138*, 13111–13114.
(16) Knie, C.; Utecht, M.; Zhao, F.; Kulla, H.; Kovalenko, S.; Brouwer, A. M.; Saalfrank, P.; Hecht, S.; Bléger, D. ortho-Fluoroazobenzenes: Visible light switches with very long-Lived Z isomers. Chemistry 2014, 20, 16492–16501.
(17) Bandara, H. M.; Burdette, S. C. Photoisomerization in different classes of azobenzene. *Chem. Soc. Rev.* **2012**, 41, 1809–1825.
(18) Sadovski, O.; Beharry, A. A.; Zhang, F.; Woolley, G. A. Spectral tuning of azobenzene photoswitches for biological applications. *Angew. Chem. Int Ed Engl* **2009**, *48*, 1484–1486.
(19) Beharry, A. A.; Sadovski, O.; Woolley, G. A. Azobenzene photoswitching without ultraviolet light. *J. Am. Chem. Soc.* **2011**, *133*, 19684–19687.
(20) Samanta, S.; Beharry, A. A.; Sadovski, O.; McCormick, T. M.; Babalhavaeji, A.; Tropepe, V.; Woolley, G. A. Photoswitching azo compounds in vivo with red light. *J. Am. Chem. Soc.* **2013**, *135*, 9777–9784.
(21) Bléger, D.; Schwarz, J.; Brouwer, A. M.; Hecht, S. o-Fluoroazobenzenes as readily synthesized photoswitches offering nearly quantitative two-way isomerization with visible light. J. Am. Chem. Soc. 2012, 134, 20597–20600.
(22) Dong, M.; Babalhavaeji, A.; Samanta, S.; Beharry, A. A.; Woolley, G. A. Red-shifting azobenzene photoswitches for in vivo use. *Acc. Chem. Res.* **2015**, *48*, 2662–2670.
(23) Dong, M.; Babalhavaeji, A.; Collins, C. V.; Jarrah, K.; Sadovski, O.; Dai, Q.; Woolley, G. A. Near-infrared photoswitching of azobenzenes under physiological conditions. *J. Am. Chem. Soc.* **2017**, *139*, 13483–13486.
(24) Lameijer, L. N.; Budzak, S.; Simeth, N. A.; Hansen, M. J.; Feringa, B. L.; Jacquemin, D.; Szymanski, W. General Principles for the Design of Visible-Light-Responsive Photoswitches: Tetra-ortho-Chloro-Azobenzenes. Angew. Chem. Int Ed Engl 2020, 59, 21663–21670.
(25) Crespi, S.; Simeth, N. A.; König, B. Heteroaryl azo dyes as molecular photoswitches. *Nat. Rev. Chem.* **2019**, *3*, 133–146.
(26) Schütt, C.; Heitmann, G.; Wendler, T.; Krahwinkel, B.; Herges, R. Design and Synthesis of Photodissociable Ligands Based on Azoimidazoles for Light-Driven Coordination-Induced Spin State Switching in Homogeneous Solution. *J. Org. Chem.* **2016**, *81*, 1206–1215.
(27) Devi, S.; Saraswat, M.; Grewal, S.; Venkataramani, S. Evaluation of Substituent Effect in Z-Isomer Stability of Arylazo-1 H-3,5-dimethylpyrazoles: Interplay of Steric, Electronic Effects and Hydrogen Bonding. *J. Org. Chem.* **2018**, *83*, 4307–4322.
(28) Heindl, A. H.; Wegner, H. A. Rational Design of Azothiophenes-Substitution Effects on the Switching Properties. *Chemistry* **2020**, *26*, 13730–13737.
(29) Gaur, A. K.; Kumar, H.; Gupta, D.; Tom, I. P.; Nampoothiry, D. N.; Thakur, S. K.; Mahadevan, A.; Singh, S.; Venkataramani, S. Structure–property relationship for visible light bidirectional photoswitchable azoheteroarenes and thermal stability of Z-isomers. *J. Org. Chem.* **2022**, *87*, 6541–6551.
(30) Naim, M. J.; Alam, O.; Nawaz, F.; Alam, M. J.; Alam, P. Current status of pyrazole and its biological activities. *J. Pharm. Bioallied Sci.* **2016**, *8*, 2–17.
(31) Alghamdi, S. S.; Suliman, R. S.; Almutairi, K.; Kahtani, K.; Aljatli, D. Imidazole as a promising medicinal scaffold: Current status and future direction. *Drug Des. Devel. Ther.* **2021**, *15*, 3289–3312.
(32) Zhang, H. Z.; Zhao, Z. L.; Zhou, C. H. Recent advance in oxazole-based medicinal chemistry. *Eur. J. Med. Chem.* **2018**, *144*, 444–492.
(33) Vitaku, E.; Smith, D. T.; Njardarson, J. T. Analysis of the structural diversity, substitution patterns, and frequency of nitrogen heterocycles among U.S. FDA approved pharmaceuticals. *J. Med. Chem.* **2014**, *57*, 10257–10274.
(34) Bhunia, S.; Dolai, A.; Samanta, S. Robust bi-directional photoswitching of thiomethyl substituted arylazopyrazoles under visible light. *Chem. Commun. (Camb)* **2020**, *56*, 10247–10250.
(35) Yang, Y.; Hughes, R. P.; Aprahamian, I. Near-infrared light activated azo-BF2 switches. J. Am. Chem. Soc. 2014, 136, 13190–13193.
(36) Weston, C. E.; Richardson, R. D.; Haycock, P. R.; White, A. J.; Fuchter, M. J. Arylazopyrazoles: Azoheteroarene photoswitches offering quantitative isomerization and long thermal half-lives. *J. Am. Chem. Soc.* **2014**, *136*, 11878–11881.
(37) Potsuki, J.; Suwa, K.; Sarker, K. K.; Sinha, C. Photoisomerization and thermal isomerization of arylazoimidazoles. *J. Phys. Chem. A* **2007**, *111*, 1403, 1403–1409.
(38) Calbo, J.; Weston, C. E.; White, A. J. P.; Rzepa, H. S.; Contreras-García, J.; Fuchter, M. J. Tuning Azoheteroarene Photoswitch Performance through Heteroaryl Design. *J. Am. Chem. Soc.* **2017**, *139*, 1261–1274.
(39) Weston, C. E.; Richardson, R. D.; Fuchter, M. J. Photoswitchable basicity through the use of azoheteroarenes. *Chem. Commun.* **2016**, *52*, 4521–4524.
(40) (a) Fang, D.; Zhang, Z. Y.; Shangguan, Z.; He, Y.; Yu, C.; Li, T. (Hetero)arylazo-1,2,3-triazoles: "Clicked" Photoswitches for Versatile Functionalization and Electronic Decoupling. *J. Am. Chem. Soc.* **2021**, *143*, 14502–14510. (b) He, Y.; Shangguan, Z.; Zhang, Z. Y.; Xie, M.; Yu, C.; Li, T. Azobispyrazole Family as Photoswitches Combining (Near-) Quantitative Bidirectional Isomerization and Widely Tunable Thermal Half-Lives from Hours to Years*. *Angew. Chem. Int Ed Engl* **2021**, *60*, 16539–16546.
(41) Tuck, J. R.; Tombari, R. J.; Yardeny, N.; Olson, D. E. A modular approach to arylazo-1,2,3-triazole photoswitches. *Org. Lett.* **2021**, *23*, 4305–4310.
(42) Slavov, C.; Yang, C.; Heindl, A. H.; Wegner, H. A.; Dreuw, A.; Wachtveitl, J. Thiophenylazobenzene: An Alternative Photoisomerization Controlled by Lone-Pair···π Interaction. *Angew. Chem. Int. Ed.* **2020**, *59*, 380–387.
(43) Kennedy, A. D. W.; Sandler, I.; Andréasson, J.; Ho, J.; Beves, J. E. Visible-light photoswitching by Azobenzazoles. *Chemistry* **2020**, *26*, 1103–1110.
(44)(a) Garcia-Amorós, J.; Maerz, B.; Reig, M.; Cuadrado, A.; Blancafort, L.; Samoylova, E.; Velasco, D. Picosecond switchable azo dyes. *Chemistry* **2019**, *25*, 7726–7732.
(45) Schehr, M.; Ianes, C.; Weisner, J.; Heintze, L.; Müller, M. P.; Pichlo, C.; Charl, J.; Brunstein, E.; Ewert, J.; Lehr, M.; Baumann, U.; Rauh, D.; Knippschild, U.; Peifer, C.; Herges, R. 2-Azo-, 2-diazocine-thiazols and 2-azo-imidazoles as photoswitchable kinase inhibitors: Limitations and pitfalls of

the photoswitchable inhibitor approach. *Photochem. Photobiol. Sci.* **2019**, *18*, 1398–1407.
(46) Matsuo, K.; Thayyil, S.; Kawaguchi, M.; Nakagawa, H.; Tamaoki, N. A visible light-controllable Rho kinase inhibitor based on a photochromic phenylazothiazole. *Chem. Commun. (Camb)* **2021**, *57*, 12500–12503.
(47) Wu, M. T.; Waksmunski, F. S.; Hoff, D. R.; Fisher, M. H.; Egerton, J. R.; Patchett, A. A. Anthelmintic 2-Arylhydrazino- and 2-Arylazo-2-thiazolines. *J. Pharm. Sci.* **1977**, *66*, 1150–1153.
(48) Whitten, D. G.; Wildes, P. D.; Pacifici, J. G.; Irick, G. Solvent and substituent on the thermal isomerization of substituted azobenzenes. Flash spectroscopic study. J. Am. Chem. Soc. 1971, 93, 2004–2008.
(49) Zhou, F.; Liu, R.; Li, P.; Zhang, H. On the properties of S···O and S···π noncovalent interactions: The analysis of geometry, interaction energy and electron density. *New J. Chem.* **2015**, *39*, 1611–1618.
(50) Motherwell, W. B.; Moreno, R. B.; Pavlakos, I.; Arendorf, J. R. T.; Arif, T.; Tizzard, G. J.; Coles, S. J.; Aliev, A. E. Noncovalent interactions of π systems with sulfur: The atomic chameleon of molecular recognition. *Angew. Chem. Int Ed Engl* **2018**, *57*, 1193–1198.
(51) The calculation result for the frontier molecular orbitals showing that the energy difference between n orbital and π* (HOMO-1 and LUMO) is larger than that between π and π* (HOMO and LUMO) seems to be inconsistent with the fact that n-π* transition band appear at lower energy region than π-π*. But this can be ascribed to the difference in exciton binding energies. see ref 40(b).
(52) Bureš, F. Fundamental aspects of property tuning in push-pull molecules. *RSC Adv.* **2014**, *4*, 58826–58851.
(53) Sharma, P. C.; Bansal, K. K.; Sharma, A.; Sharma, D.; Deep, A. Thiazole-containing compounds as therapeutic targets for cancer therapy. *Eur. J. Med. Chem.* **2020**, *188*, 112016.

Table of Contents (TOC)